Lipid Loading of Human Vascular Smooth Muscle Cells Induces Changes in Tropoelastin Protein Levels and Physical Structure

Valerie Samouillan,[†*] Jany Dandurand,[†] Laura Nasarre,[‡] Lina Badimon,[‡] Colette Lacabanne,[†] and Vicenta Llorente-Cortés[‡*]

[†]Physique des Polymères, Institut Carnot, CIRIMAT UMR 5085, Université Paul Sabatier, Tolouse, France; and [‡]Cardiovascular Research Center, CSIC-ICCC, IIB-Sant Pau, Hospital de la Santa Creu i Sant Pau, Barcelona, Spain

ABSTRACT Aggregated low-density lipoprotein (agLDL), one of the main LDL modifications in the arterial intima, contributes to massive intracellular cholesteryl ester (CE) accumulation in human vascular smooth muscle cells (VSMC), which are major producers of elastin in the vascular wall. Our aim was to analyze the levels, physical structure, and molecular mobility of tropoelastin produced by agLDL-loaded human VSMC (agLDL-VSMC) *versus* that produced by control VSMC. Western blot analysis demonstrated that agLDL reduced VSMC-tropoelastin protein levels by increasing its degradation rate. Moreover, our results demonstrated increased levels of precursor and mature forms of cathepsin S in agLDL-VSMC. Fourier transform infrared analysis revealed modifications in the secondary structures of tropoelastin produced by lipid-loaded VSMCs. Thermal and dielectric analyses showed that agLDL-VSMC tropoelastin has decreased glass transition temperatures and distinct chain dynamics that, in addition to a loss of thermal stability, lead to strong changes in its mechanical properties. In conclusion, agLDL lipid loading of human vascular cells leads to an increase in cathepsin S production concomitantly with a decrease in cellular tropoelastin protein levels and dramatic changes in secreted tropoelastin physical structure. Therefore, VSMC-lipid loading likely determines alterations in the mechanical properties of the vascular wall and plays a crucial role in elastin loss during atherosclerosis.

INTRODUCTION

The synthesis of elastin, the main extracellular matrix protein in the media of the arterial and aortic walls, occurs during late fetal and early postnatal life and stops in the aortic tissue of adults (1). One of the mechanisms that contribute to the lack of elastin synthesis in adults is the rapid degradation of elastin mRNA through the action of specific miRNA (2). Although mature elastic fibers are extremely stable in humans (3,4), a progressive loss of vascular elastin content leading to increased vascular stiffening occurs in aging (5,6) and atherosclerosis (7,8).

Vascular smooth muscle cells (VSMCs), the main cellular component of the vascular wall, are also the major producers of tropoelastin, the soluble precursor of elastin. However, VSMCs in atherosclerotic lesions are unable to produce normal elastic fibers (9) due to atherosclerotic risk factors such as diabetes and associated hyperglycemia, endothelial dysfunction, and inflammation (10,11). It is known that experimental hypercholesterolemia decreases the elastin content of the wall in vivo (12) and in in vitro systems (13). However, the role of hypercholesterolemia in the altered elastogenic capacity of VSMCs and the possible mechanisms involved are almost completely unknown. Accumulation of extracellular matrix-retained low-density lipoproteins (LDL) in the arterial intima is crucial for the onset and progression of atherosclerosis (14,15). The incorporation of matrix-retained LDL by macrophages (16,17) and VSMC (18,19) leads to the accumulation of cholesteryl ester (CE) and formation of foam cells. Macrophages become foam cells through the uptake of diversely modified LDLs, whereas the aggregation of LDLs seems to be a key condition for lipid accumulation in VSMCs (21–23). Aggregated LDLs (agLDLs) obtained by vortexing LDL in vitro share structural characteristics with LDL aggregates present in atherosclerotic lesions (24). Our previous results showed that hypercholesterolemia can increase the capacity of VSMCs to take up LDL from the intima by regulating cellular LDL receptor-related protein 1 (LRP1) (25), the receptor for agLDL uptake in human VSMCs (18). Intracellular cholesterol accumulation alters proteoglycan composition (26) and collagen assembly (27) in VSMCs. However, it is unknown whether intracellular lipid can change the levels or the physical characteristics of the tropoelastin synthesized by human VSMCs.

Tropoelastin contains glycine amino acids (28), which account for one-third of its composition, and several lysine derivatives that serve as covalent cross-links between protein monomers (29). Elastin can be thus considered as a three-dimensional network with 60–70 amino acids between two cross-linking points, with the alternation of hydrophilic cross-linking domains and dynamic hydrophobic domains with fluctuating turns, buried hydrophobic residues, and main-chain polar atoms forming hydrogen (H)-bonds with water (30–33). This peculiar molecular architecture determines its elastic properties, insolubility, and resistance to proteolysis (34). Our goal in this work was to analyze tropoelastin levels and the physical structure and molecular mobility of tropoelastin produced by

Submitted March 14, 2012, and accepted for publication June 20, 2012.

*Correspondence: valerie.samouillan@univ-tlse3.fr or cllorente@csic-iccc.org

Editor: Edward Egelman.

0006-3495/12/08/0532/9 $2.00

http://dx.doi.org/10.1016/j.bpj.2012.06.034

agLDL-lipid-loaded human VSMCs in comparison with that produced by control VSMCs.

For this purpose, we combined cellular and molecular biology techniques with polymer characterization techniques that were previously shown to be efficient for assessing the molecular architecture and chain dynamics of proteins (35–37).

MATERIALS AND METHODS

Cellular and molecular biology techniques

Human VSMCs

Primary cultures of human VSMCs were obtained from nonatherosclerotic areas of human coronary arteries from hearts explanted during heart transplantation at the Hospital of Santa Creu i Sant Pau as previously described (18,19). The transplanted patients were men between the ages of 40 and 60 years. The explants were incubated at 37°C in a humidified atmosphere of 5% CO_2. Cells grown from the explants were suspended in a solution of trypsin/EDTA and subcultured. They grew in monolayers in medium 199 supplemented with 20% fetal calf serum and 2% human serum, 2 mmol/L L-glutamine, 100 U/mL penicillin G, and 100 μg/mL streptomycin (GIBCO Laboratories, Gaithersburg, MD). The study was approved by the institutional ethics committee of the Hospital of Santa Creu i Sant Pau and conducted in accordance with the Declaration of Helsinki.

LDL isolation and modification

Human LDL ($d_{1.019}$-$d_{1.063}$ g/mL) was obtained from the pooled sera of normocholesterolemic volunteers by sequential ultracentrifugation. The LDLs were dialyzed and LDL protein concentration was determined according to the bicinchoninic method, and cholesterol concentration was determined with the use of a commercial kit (Roche Molecular Biochemical, Boulogne-Billancourt, France). The LDLs used in the experiments were <48 h old. The purity of the LDLs was assessed by agarose gel electrophoresis (Paragon system; Beckmann Coulter, Brea, CA) (18,19).

AgLDLs were prepared by vortexing LDLs in phosphate-buffered saline (PBS) at room temperature. The formation of LDL aggregates by vortexing was monitored by measuring the turbidimetry (absorbance at 680 nm) as previously described (18,19). The precipitable fraction of particles obtained by vortexing was similar in size to the largest particles obtained by incubation with versican (19).

Determination of intracellular free CE and triglyceride content

VSMCs were incubated with agLDL (50 μg/mL) for 15 days. After the lipoprotein incubation was completed, the cells were exhaustively washed (twice with PBS, twice with PBS-1% BSA, and twice with PBS-1% BSA-heparin 100 U/mL) before they were harvested into 1 mL of 0.15 mol/L NaOH. Lipid extraction was performed as previously described (18,19). Three different concentrations of standards (a mixture of cholesterol and cholesterol palmitate) were applied to thin-layer chromatography plates. Spots corresponding to free cholesterol (FC), triglycerides, and CE in the thin-layer chromatography were quantified by densitometry against the standard curve of cholesterol, triglycerides, and cholesterol palmitate, respectively, using a computing densitometer (Phosphorimager model 445 SI; Molecular Dynamics, Sunnyvale, CA).

Determination of elastin gene expression by real-time polymerase chain reaction

Total RNA was isolated by Tripure isolation reagent (Roche Molecular Biochemicals) according to the manufacturer's protocol. Tropoelastin mRNA expression levels were determined by real-time polymerase chain reaction (PCR; Life Technologies, Foster City, CA) using Assays-on-Demand (Hs00355783_m1; Applied Biosystems, Foster City, CA). Human *gapdh* (4326317E; Applied Biosystems) was used as internal control, and PCR was performed on the ABIPRISM7000 detection system. The threshold cycle (Ct) values were determined and normalized to the housekeeping gene.

Western blot analysis

Blots were incubated with monoclonal antibodies against human elastin (sc-166369, dilution 1:50; Santa Cruz Biotechnology, Santa Cruz, CA) or with monoclonal antibodies against human cathepsin (sc-271619; dilution 1:100; Santa Cruz Biotechnology). Elastin (F-5) is a mouse monoclonal antibody raised against amino acids 431–730 of elastin of human origin, and cathepsin S (E-3) is a mouse monoclonal antibody that is specific for an epitope mapping between amino acids 302 and 331 at the C-terminus of cathepsin S of human origin, and recognizes precursor (37 KDa) and mature (24 KDa) cathepsin S. To test equal protein loading for the different samples, blots were also incubated with monoclonal antibodies against human β-actin (ab8226-100, dilution 1:5000; Abcam Biochemicals, Cambridge, MA). The antibodies used for Western blotting detected cellular but not secreted tropoelastin.

Measurement of cellular tropoelastin protein stability in control and lipid-loaded VSMCs

To measure the stability of tropoelastin protein in human VSMCs, we preexposed the cells to agLDL (50 μg/mL) for 48 h. Cycloheximide (100 μmol/L) was then added and cell cultures were harvested at various time points after cycloheximide treatment (12, 24, and 48 h), and collected in lysis buffer. The protein was then processed for Western blot analysis. The stability of the tropoelastin protein was assessed according to the proportion of the initial protein that remained after cycloheximide treatment.

Physical techniques

For physical techniques, cell supernatants were centrifuged to remove lipids that were not taken up by the cells and cellular debris. The samples were then freeze-dried before tropoelastin physical characterizations were obtained. Fourier transform infrared analysis (FTIR), thermogravimetric analysis (TGA), differential scanning calorimetry (DSC), and dynamic dielectric spectrometry (DDS) are described in the Supporting Material.

RESULTS AND DISCUSSION

Fig. 1 shows that agLDL (50 μg/mL, 15 days) induced a strong intracellular accumulation of CEs in a dose-dependent manner in human VSMCs, consistent with the high capacity of agLDL to induce foam cell formation from VSMCs previously described by our group (18,19).

Real-time PCR results (Fig. 2) demonstrated that control and lipid-loaded VSMCs showed the same pattern of tropoelastin mRNA expression with time. The lack of effect of agLDL on tropoelastin mRNA expression suggests that agLDL influences a protein's expression levels by modulating its degradation. To assess whether agLDL could influence tropoelastin protein stability, we preexposed human VSMCs to agLDL followed by addition of cycloheximide, an inhibitor of translation. As shown in Fig. 3, the percentage of initial cellular tropoelastin protein remained constant in the control VSMCs. In contrast, cellular

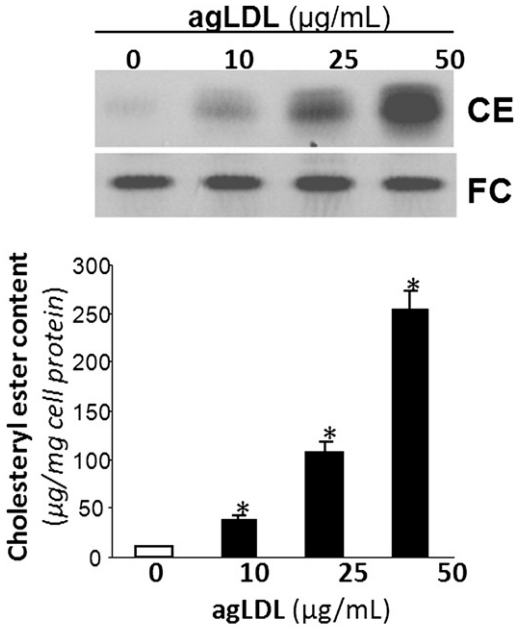

FIGURE 1 VSMCs were exposed to increasing concentrations (10, 25, and 50 μg/mL) of agLDL for 15 days. Cells were then collected and lipid extraction was performed as explained in Materials and Methods. Thin-layer chromatography shows intracellular CE and FC bands. Results are expressed as micrograms of cholesterol per milligram of protein, and are shown as the mean ± SE of three experiments performed in duplicate. $^*p < 0.05$, versus control VSMC.

tropoelastin levels decayed by ~40% in VSMCs exposed to agLDL for 48 h. These findings suggest that lipid loading modulates the half-life of tropoelastin in human VSMCs. In fact, cellular tropoelastin protein levels were significantly downregulated in VSMC exposed to agLDL for 48 h (agLDL: 35.98 ± 0.75 a.u. vs. 67.34 ± 3.23 a.u., $p < 0.05$) and 96 h (agLDL: 4.71 ± 0.66 a.u. vs. 63.18 ± 5.65 a.u., $p < 0.05$) (Fig. 4, *A* and *B*), consistently with the downregulatory effects of hypercholesterolemia on aortic elastin levels in in vivo models (12,13). In contrast, cellular tropoelastin protein levels were not altered during the test days in control VSMCs. Elastic tissue is the most stable component of the vascular wall, and therefore the lower VSMC tropoelastin contribution by lipid-loaded VSMC could be negligible for the extracellular matrix. Remarkably, in atherosclerosis, a progressive loss of existing elastic fibers occurs as a result of different cardiovascular risk factors, and most defects in the progression of vascular elastin loss are associated with enzymatic degradation. Our results show that agLDL (50 μg/mL, 96 h) significantly increased both cellular precursor (Fig. 4, *A* and *C*) and mature (Fig. 4, *A* and *D*) forms of cathepsin S by 21- and 4-fold, respectively. Cathepsin S has a potent elastolytic activity (38), and therefore the degradative capacity of lipid-loaded VSMC likely plays a role in the degradation of existing elastic tissue during atherosclerotic progression. It was previously reported that cathepsin S is overexpressed in SMCs of atherosclerosis and neointimal lesions in humans and animals, and that cathepsin-S-deficient animals showed reduced fragmentation of elastic lamina in aortas of atherosclerotic lesions (39). Taken together, these results point to lipid-loaded VSMCs as crucial players in the loss of elastin that occurs during atherosclerosis.

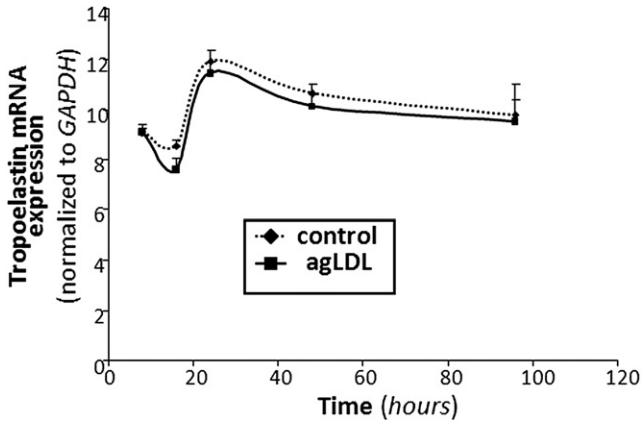

FIGURE 2 VSMCs were exposed to agLDL (50 μg/mL) for increasing periods of time (8, 16, 24, 48, and 96 h). Real-time PCR quantification of tropoelastin mRNA levels was performed. Data were processed with a specially designed software program based on Ct values, normalized to GAPDH mRNA, and expressed as the mean ± SE of three independent experiments performed in duplicate.

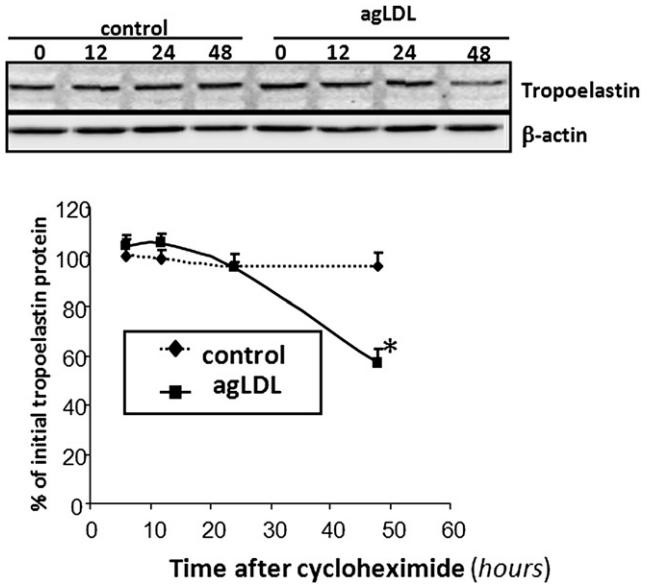

FIGURE 3 VSMCs were preexposed to agLDL (50 μg/mL) for 48 h, followed by incubation with cycloheximide (100 μmol/L) for the indicated times. Unchanged levels of β-actin are shown as loading control. Line graphs show the percentage of the value before the addition of cycloheximide. Results are expressed as the mean ± SE of two independent experiments performed in triplicate. $^*p < 0.05$ versus control VSMC.

We identified FTIR/ATR absorption bands (Fig. 5) of purified supernatant fractions using bibliographic data on elastin (40,41), tropoelastin (42,43), κ-elastins (40,44), and

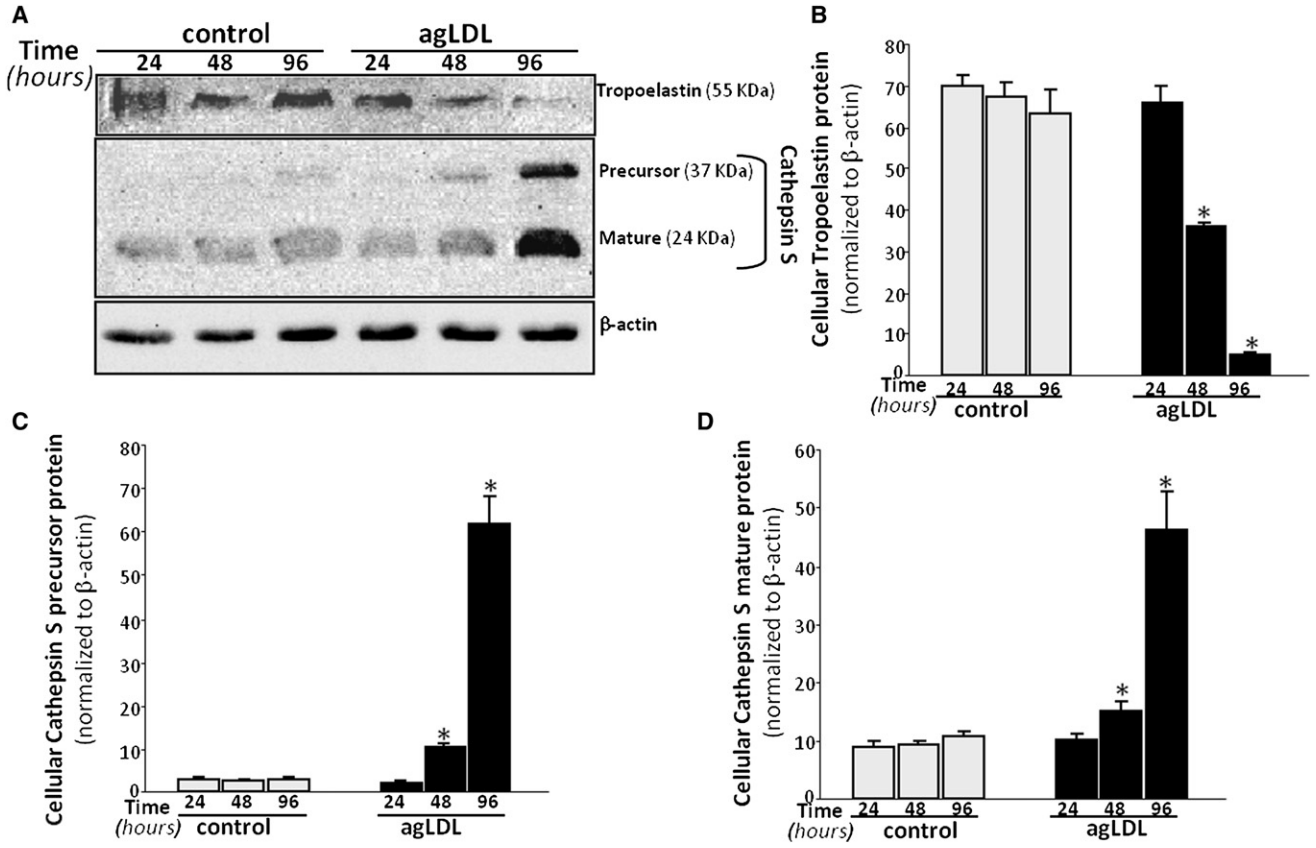

FIGURE 4 VSMCs were exposed to agLDL (50 μg/mL) for increasing periods of time (24, 48, and 96 h). (*A*) Representative Western blot analysis showing the time-course of tropoelastin and precursor and mature cathepsin S protein bands in VSMCs exposed to agLDL. Unchanged levels of β-actin are shown as loading control and used to normalize the tropoelastin and cathepsin S bands. Bar graphs show the quantification of tropoelastin (*B*), and precursor (*C*) and mature (*D*) cathepsin S bands in control and agLDL-loaded VSMCs. Data are expressed as mean $\pm$ SE of three independent experiments performed in duplicate. *$p < 0.05$ versus control VSMC.

synthetic polypeptides with recurrent sequences of tropoelastin exons (45,46), and general data on protein FTIR absorption bands (47,48). The probable band assignments are shown in Table S1.

The classical absorption bands of proteins (amides A, I, II, and III) are found on the two spectra, and their positions are consistent with the literature data on tropoelastin. The two fractions of supernatants exhibit quite similar profiles, suggesting very similar chemistry. As shown in Table S2, the agLDL FTIR spectrum fits very well with literature data (33), with the very specific absorption of the carbonyl stretching of ester bond at 1734 cm^{-1}.

We can observe a slight shoulder at 1734 cm^{-1} in the spectrum of supernatant from agLDL-VSMC, indicating that a weak fraction of agLDL could remain after the purification, and suggesting an interaction between tropoelastin and agLDL, as previously reported for tropoelastin and LDL (49).

To obtain more information about the secondary structures of tropoelastin, we resolved the amide I region of the supernatant from control VSMC using the Fourier Self Deconvolution (FSD) procedure (42,50). As shown in Fig. 5 *B*, it resulted in six components that are the signatures of the different conformations of the protein at 1693 cm^{-1} (antiparallel β-sheets) (40–43,45,51), 1679 cm^{-1} (antiparallel β-sheets and β-turns) (41,42,44), 1657 cm^{-1} (irregular structures/unordered conformations) (43,45,52) or undefined component (40), 1644 cm^{-1} (α-helices) (42,43,53), 1632 cm^{-1} (β-sheets) (41–45,53), and 1617 cm^{-1} (β-sheets) (42,43,53). Assuming that the area of the different bands is correlated to the proportion of each kind of conformation, a quantitative estimation performed on the initial decomposed amide I region (with the maxima of the peaks fixed from the FSD treatment) leads to ~8% of α-helices, 46% of β-structures, and 46% of unordered/undefined conformations, which is very close to previously published data for human elastin (40). The presence of unordered conformations is confirmed by the vibration at 1542 cm^{-1} in the amide II band (45,46), and the presence of β-structures is confirmed by the vibration at 1515 cm^{-1} (44–46). The band located at 1591 cm^{-1} was not associated with the particular structure of tropoelastin and may be associated with another component. Nevertheless, such a band can be also observed in tropoelastin samples in the literature (50).

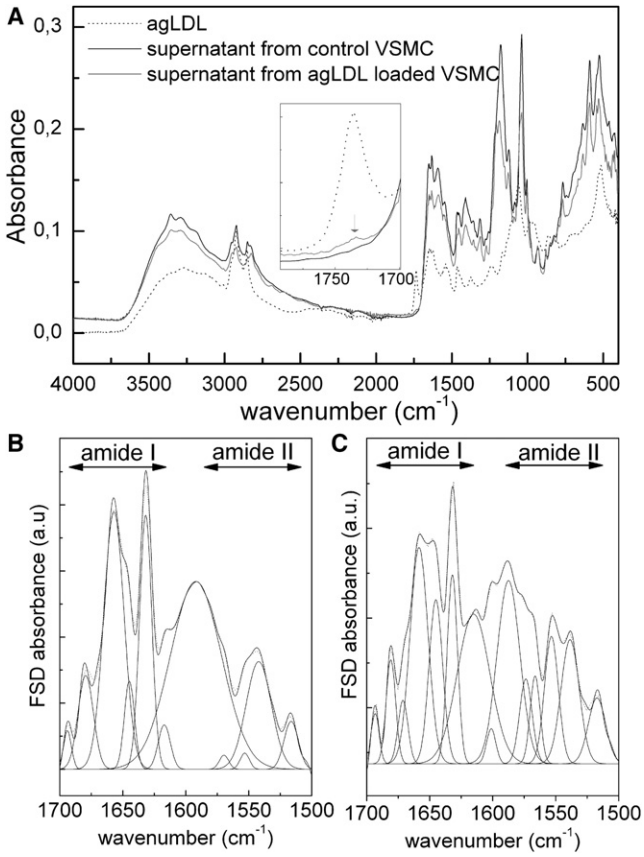

FIGURE 5 FTIR/ATR spectra of purified supernatants (from control VSMC and agLDL-loaded VSMC) and pure agLDL (*A*). FSD trace and decomposition at 1700–1500 cm^{-1} for supernatant from control VSMCs (*B*) and agLDL-loaded VSMCs (*C*).

In the case of the supernatant from agLDL-VSMC, the decomposition of the amide I band by the FSD protocol presented in Fig. 5 *C* yielded seven components at 1693 cm^{-1} (antiparallel β-sheets), 1680 cm^{-1} (antiparallel β-sheets and β-turns), 1667 cm^{-1}, 1657 cm^{-1} (irregular structures/unordered conformations), 1646 cm^{-1} (α-helices), 1632 cm^{-1} (β-sheets) and 1613 cm^{-1} (β-sheets). By analogy to previous results, the appearance of the vibration at 1667 cm^{-1} could be attributed to irregular structures (40,43); to another, undefined component (52); or to non-H-bonded groups (45). This assumption is confirmed by the intensification of the vibration band at 1555 cm^{-1} in the amide II region, attributed to non-H-bonded groups.

Thermogravimetric (TG) and derivative thermogravimetric (DTG) plots of purified supernatants from control VSMCs and from agLDL-VSMCs are presented in Fig. 6. The mass decrement during the heating process was determined from the TG curves, and the temperature of the maximum speed of the process (T_{max}) was determined from the maximum of the DTG curves. The corresponding thermal parameters for both samples are listed in Table S3.

The global trend of the two TG plots corresponds to the classical thermal behavior of freeze-dried proteins (54).

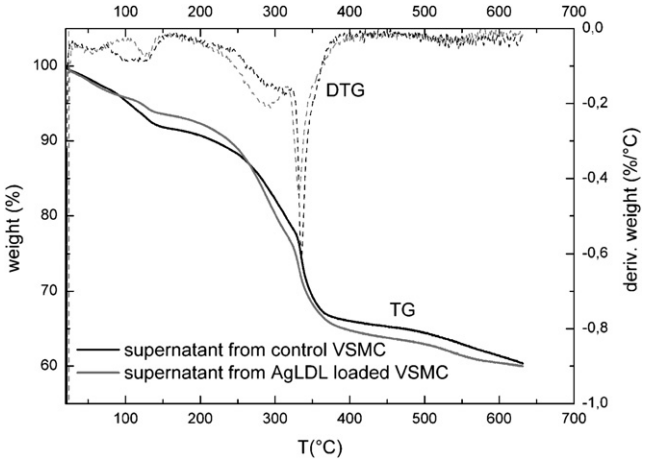

FIGURE 6 TGA and DTG of purified supernatants from control VSMCs and agLDL-loaded VSMCs.

The first stage (between 25°C and 100°C) is connected to the evaporation of water absorbed to the protein, and corresponds to 8.2% and 6.4% of the total mass for control and agLDL-VSMC samples, respectively, meaning that freeze-dried elastin material from agLDL-VSMC is more hydrophobic than that from control VSMC.

The second stage is associated with a multistep stage corresponding to the degradation of the sample, namely, a deamination and depolymerization arising from the breaking of polypeptidic bonds. The degradation in two well-marked steps could be due to the presence of both fractions of tropoelastin in the supernatants, with the second (aggregated one) degrading at higher temperatures. Elastic material from the agLDL-VSMCs began to degrade at lower temperatures than the control elastic material, suggesting that the thermal stability of tropoelastin and aggregated tropoelastin are altered when VSMCs are loaded with agLDL.

Superimposed on Fig. 7 are the two thermograms corresponding to the first and second scans of purified supernatants recorded at 20°C/min between 30°C and 180°C, and −60°C and 250°C, respectively. In accordance with previous studies (42,54), the first scan performed between 30°C and 180°C is characteristic of water-protein interactions, and generally presents the feature of a broad endothermic peak associated with the departure of bound water. The broadness of the peak can be explained by the complexity of the transition, which must include disruption of protein-water interactions, evaporation, and vaporization (54–56). The enthalpy associated with this transition is connected to the water content of the supernatant: the largest value of the enthalpy is found for supernatants from control VSMCs (160J/g vs. 120 J/g), which means that this fraction corresponds to the more-hydrated sample in accordance with TGA data. Superimposed on this broad transition are other events that can be associated with the thermal answer of proteins. The second scans

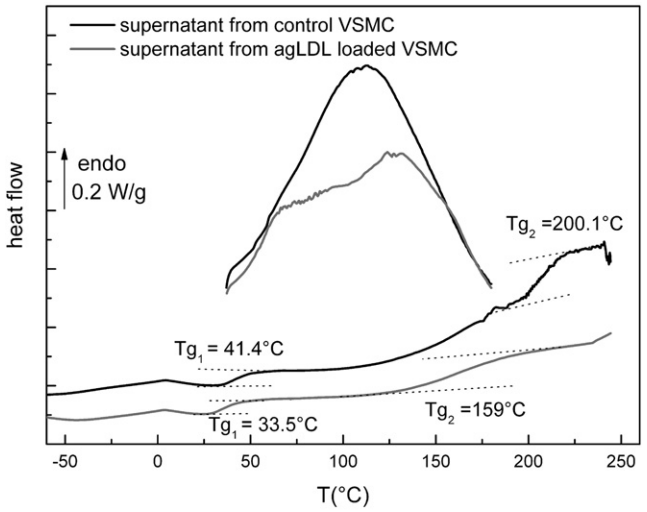

FIGURE 7 Second DSC thermograms of purified supernatants from control and agLDL-loaded VSMCs.

performed between −60°C and 250°C show the specific characteristics of dehydrated proteins (50,54). Two major glass transitions are observed for the two samples as a step of the heat flow (the glass transition temperatures T_g are reported in the graph).

The presence of two glass transitions is indicative of two kinds of amorphous phases in the purified supernatants, and corroborates the TGA measurements showing different stabilities of tropoelastin. According to literature data, the only transition that is detectable for native elastin and tropoelastin is a glass transition, namely, a pseudo-second-order transition due to the transition from a glassy to a rubber state at ~200°C for dehydrated elastin and tropoelastin (42,50,54,57,58). Elastin does not possess a long-range order, and although different secondary conformations can be found in this protein, it can be considered as amorphous for the physical structure, which is in good agreement with the model of labile, dynamic β-turns in hydrophobic domains proposed by Debelle and Tamburro (31) and Tamburro et al. (32), and Li et al.'s (59) model that describes hydrophobic domains of elastin as compact amorphous structures.

In accordance with these previous studies, the second glass transition (at $T_{g2} = 200.1°C$) of supernatant from control VSMCs could be attributed to the thermal characteristics of aggregated tropoelastin. The lower glass transition (at $T_{g1} = 41.4°C$) could be attributed to nonaggregated tropoelastin. In the case of supernatant from agLDL-VSMC, both tropoelastin and aggregated tropoelastin undergo a glass transition at lower temperature, with a spectacular decrease of the glass transition associated with aggregated tropoelastin ($T_{g2} = 159°C$). This phenomenon could be due to an interaction between agLDL and tropoelastin, as evidenced by the weak specific FTIR absorption band of agLDL in supernatant from agLDL-loaded VSMCs.

Superimposed on Fig. 8, *A* and *B*, are the isotherms of tan δ recorded for supernatant from control VSMCs in different temperature ranges. The experiments were stopped at 100°C because a substantial conductivity at higher temperatures was hiding possible dipolar relaxations.

In this temperature range, three modes can be observed and associated with dipolar relaxations. The lower temperature mode (Fig. 8 *A*) is observed from −70°C to −30°C and labeled β-mode by analogy with previous works on proteins (58–61); the higher temperature mode (Fig. 8 *B*) is observed between 5°C and 60°C and labeled α-mode. A minor intermediate mode (not shown) is observed as a shoulder at −15°C and −10°C and labeled α'-mode. For each temperature, the frequency of the maximum is noted, and the associated relaxation time τ(T) is computed using the following formula:

$$\tau(\mathrm{T}) = \frac{1}{(2\pi \mathrm{f}_{\max})}. \quad (1)$$

The temperature dependence of the dipolar modes can be reached by plotting the variation of τ(T) versus temperature. In Fig. 9 *A*, we plot the variation of the relaxation times in a logarithmic scale versus temperature in an offset reciprocal scale for the α-, α'-, and β-modes of supernatant from control VSMCs.

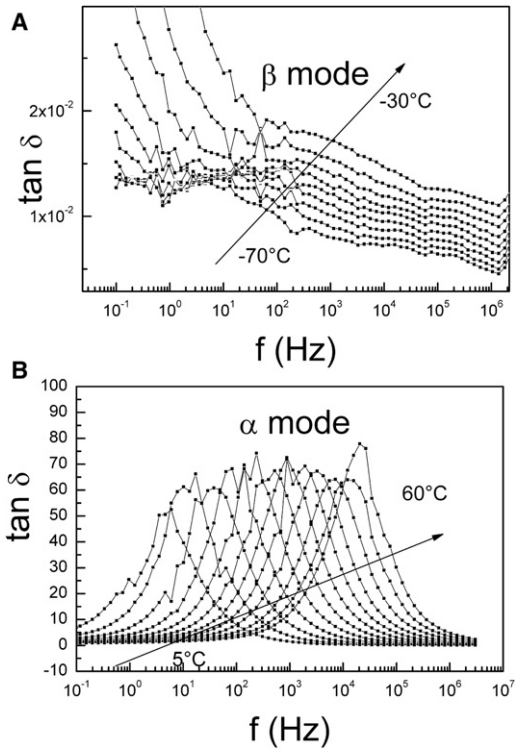

FIGURE 8 DDS isotherms of purified supernatant from control VSMCs. (*A*) The β-mode between −70°C and −30°C. (*B*) The α-mode between 5°C and 60°C.

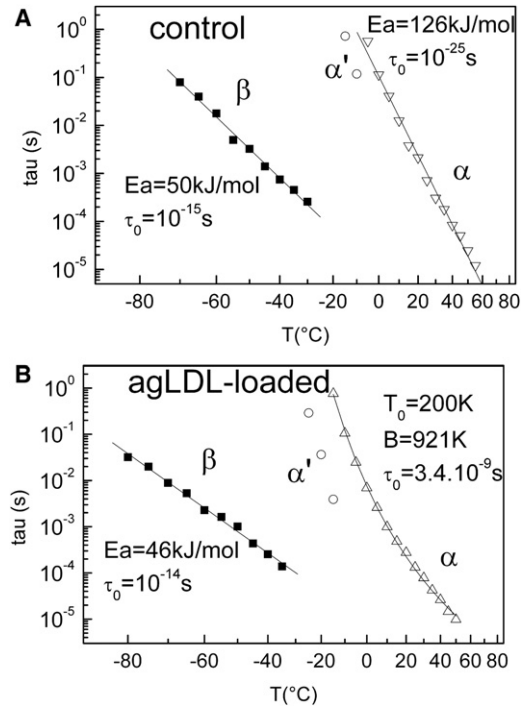

FIGURE 9 Temperature dependence of the three dipolar modes of purified supernatant from control VSMCs (*A*) and agLDL-loaded VSMCs (*B*).

A linear relationship is obtained for the β- and α-modes, revealing that τ(T) follows an Arrhenius law:

$$\tau(\mathrm{T}) = \tau_0 \exp\left(\frac{\mathrm{Ea}}{\mathrm{RT}}\right), \quad (2)$$

where τ_0 is the preexponential factor, R is the gas constant, and Ea is the activation energy.

The corresponding values computed from a linear fit are reported in Fig. 9 *A*.

The values of τ_0 (10^{-15} s) and Ea (50 kJ·mol^{-1}) of the β-mode are typical of the classical and universal secondary process in proteins (62): the value of the activation energy corresponds to the energy required to break two H-bonds, allowing the further reorientation of the dipole. The preexponential factor τ_0 is associated with the activation entropy ΔS in Eyring's equation:

$$\tau_0 = \frac{\mathrm{h}}{(\mathrm{kT})} \exp\left(\frac{-\Delta \mathrm{S}}{\mathrm{R}}\right), \quad (3)$$

where h is Planck's constant and k is Boltzmann's constant.

The value of 10^{-15} s corresponds to a weak activation entropy (ΔS $\approx$40 J·K^{-1}·mol^{-1}) and is indicative of a small cooperative mode. The β-mode can be thus associated with the dipolar relaxation of carbonyl groups of the protein bound to water (60).

As for the α-mode, the values of τ_0 (10^{-25} s) and Ea (126 kJ·mol^{-1}) are characteristic of the main process in proteins: the preexponential factor corresponds to an important activation entropy (ΔS $\approx$234 J·K^{-1}·mol^{-1}), indicative of a cooperative mode (63), and the α-mode is thus associated with the dielectric manifestation of the first glass transition of tropoelastin (observed by DSC at Tg_1= 41.4°C), implying motions of some tens of nanometers along the polypeptidic backbone. Because the α-process has an Arrhenius-like behavior, tropoelastin possesses a strong network of H-bonds, as previously observed for different fibrous proteins (35).

The same dielectric protocol was applied to supernatant from agLDL-loaded VSMCs. As with the control sample, three relaxation modes labeled β, α, and α' were observed in this temperature range. The logarithmic variation of the relaxation time τ(T) versus temperature is plotted for each mode in Fig. 9 *B*.

As with the control sample, the relaxation time of the β-mode has an Arrhenius-like temperature dependence. The values of the Arrhenius parameters reported in Fig. 9 *B* are roughly similar, meaning that the localized motions along the backbone of tropoelastin are roughly the same for the two supernatants.

The α-mode that was previously associated with the tropoelastin glass transition is shifted toward low temperature (~10°C), in accordance with the DSC results. Moreover, the temperature dependence of the relaxation time follows a Vogel-Fulcher-Tamman (VFT) behavior, in contrast to the Arrhenius-like behavior observed for the relaxation time of control tropoelastin. The corresponding function is written as

$$\tau(\mathrm{T}) = \tau_0 \exp\left(\frac{\mathrm{B}}{(\mathrm{T} - \mathrm{T}_0)}\right). \quad (4)$$

The corresponding values of τ_0, B, and T_0 are reported in Fig. 9, *A* and *B*.

The important discrepancy observed between the delocalized motions along the polypeptidic backbone of tropoelastin from control and agLDL-loaded VSMCs can be interpreted in terms of differences between the H-bond network density of the two systems: In a general way, an Arrhenius-like behavior is connected to a strong H-bond network, whereas a VFT-like behavior is attributed to a more loosely bound H-bond network (50). These results suggest that tropoelastin possesses more non-H-bonded groups when VSMCs are agLDL-loaded, as previously shown by FTIR. This could be due in part to the interaction between agLDL and tropoelastin (as revealed by FTIR analysis) modifying its secondary structure and aggregation.

CONCLUSION

Aggregation of LDL is one of the main mechanisms by which VSMCs become foam cells during atherosclerosis; however, the role played by agLDL in the inability of

VSMCs to produce normal elastic fibers in atherosclerosis is almost completely unknown. Here, we show that agLDL loading reduced the cellular elastogenic capacity and increased the elastolytic potential of human VSMCs. The physical analysis showed modifications of secreted tropoelastin when VSMCs were agLDL-loaded. First, the affinity with water was decreased, suggesting a loss of elasticity because water is essential for the elasticity of elastin. At the conformational level, the results revealed a new (to our knowledge), undefined, probably non-H-bonded structure for tropoelastin that could be due to an interaction of the protein with remaining agLDL, inducing the distinct chain dynamics of tropoelastin evidenced by dielectric analysis and the decrease of the glass transition of tropoelastin and aggregated tropoelastin. These alterations in the physical structure of tropoelastin will unfailingly induce alterations in the mechanical properties of elastic fibers, in particular a loss of the rubber-like properties and a loss of the reversibility during deformations that may favor the rupture of the macromolecule. Indeed, the increased degradative capacity of agLDL-loaded VSMCs may contribute to the physical alterations of secreted tropoelastin. Moreover, the degradative capacity of lipid-loaded VSMCs may play a role in the degradation of existing elastic tissue during atherosclerotic progression.

Taken together, our results suggest that VSMC intracellular lipids provoke crucial alterations in cellular tropoelastin levels, mechanical properties, and capacity to break down elastin. Moreover, our results point to lipid-loaded VSMCs as crucial players in the loss of elastin during atherosclerosis.

SUPPORTING MATERIAL

Fourier transform infrared analysis, thermogravimetric analysis, differential scanning calorimetry, and dynamic dielectric spectrometry plus three tables are available at http://www.biophysj.org/biophysj/supplemental/S0006-3495(12)00723-0.

This work was supported by grants from Red de Investigación en Insuficiencia Cardiaca (RD06/0003/0015) and Fondo de Investigaciones Sanitarias, Instituto Salud Carlos III (PI11/00747), cofinanced by Fondo Europeo de Desarrollo Regional, MARATON TV3-Malalties Cardiovasculars.

REFERENCES

1. Johnson, D. J., P. Robson, …, F. W. Keeley. 1995. Decreased elastin synthesis in normal development and in long-term aortic organ and cell cultures is related to rapid and selective destabilization of mRNA for elastin. *Circ. Res.* 77:1107–1113.
2. Ott, C. E., J. Grünhagen, …, P. N. Robinson. 2011. MicroRNAs differentially expressed in postnatal aortic development downregulate elastin via 3′ UTR and coding-sequence binding sites. *PLoS ONE.* 6:e16250.
3. Shapiro, S. D., S. K. Endicott, …, E. J. Campbell. 1991. Marked longevity of human lung parenchymal elastic fibers deduced from prevalence of D-aspartate and nuclear weapons-related radiocarbon. *J. Clin. Invest.* 87:1828–1834.
4. Powell, J. T., N. Vine, and M. Crossman. 1992. On the accumulation of D-aspartate in elastin and other proteins of the ageing aorta. *Atherosclerosis.* 97:201–208.
5. Mitchell, G. F., H. Parise, …, D. Levy. 2004. Changes in arterial stiffness and wave reflection with advancing age in healthy men and women: the Framingham Heart Study. *Hypertension.* 43:1239–1245.
6. Fritze, O., B. Romero, …, U. A. Stock. 2012. Age-related changes in the elastic tissue of the human aorta. *J. Vasc. Res.* 49:77–86.
7. Farrar, D. J., M. G. Bond, …, J. K. Sawyer. 1991. Anatomic correlates of aortic pulse wave velocity and carotid artery elasticity during atherosclerosis progression and regression in monkeys. *Circulation.* 83:1754–1763.
8. Wang, Y. X., M. Halks-Miller, …, K. Kauser. 2000. Increased aortic stiffness assessed by pulse wave velocity in apolipoprotein E-deficient mice. *Am. J. Physiol. Heart Circ. Physiol.* 278:H428–H434.
9. Saulnier, J. M., M. Hauck, …, J. M. Wallach. 1991. Human aortic elastin from normal individuals and atherosclerotic patients: lipid and cation contents; susceptibility to elastolysis. *Clin. Chim. Acta.* 200:129–136.
10. Fox, C. S., S. Coady, …, P. J. Savage. 2007. Increasing cardiovascular disease burden due to diabetes mellitus: the Framingham Heart Study. *Circulation.* 115:1544–1550.
11. Cernes, R., R. Zimlichman, and M. Shargorodsky. 2008. Arterial elasticity in cardiovascular disease: focus on hypertension, metabolic syndrome and diabetes. *Adv. Cardiol.* 45:65–81 (Review).
12. Augier, T., P. Charpiot, …, D. Garçon. 1997. Medial elastic structure alterations in atherosclerotic arteries in minipigs: plaque proximity and arterial site specificity. *Matrix Biol.* 15:455–467.
13. Csonka, E., K. Szemenyei, …, A. M. Robert. 1980. Morphological examination of aortic endothelial and smooth muscle cells grown in vitro on collagen membranes. *Artery.* 8:253–258.
14. Steinberg, D., S. Parthasarathy, …, J. L. Witztum. 1989. Beyond cholesterol. Modifications of low-density lipoprotein that increase its atherogenicity. *N. Engl. J. Med.* 320:915–924.
15. Camejo, G., E. Hurt-Camejo, …, G. Bondjers. 1998. Association of apo B lipoproteins with arterial proteoglycans: pathological significance and molecular basis. *Atherosclerosis.* 139:205–222.
16. Morton, R. E., G. A. West, and H. F. Hoff. 1986. A low density lipoprotein-sized particle isolated from human atherosclerotic lesions is internalized by macrophages via a non-scavenger-receptor mechanism. *J. Lipid Res.* 27:1124–1134.
17. Hoff, H. F., and J. O'Neil. 1991. Lesion-derived low density lipoprotein and oxidized low density lipoprotein share a lability for aggregation, leading to enhanced macrophage degradation. *Arterioscler. Thromb.* 11:1209–1222.
18. Llorente-Cortés, V., J. Martínez-González, and L. Badimon. 2000. LDL receptor-related protein mediates uptake of aggregated LDL in human vascular smooth muscle cells. *Arterioscler. Thromb. Vasc. Biol.* 20:1572–1579.
19. Llorente-Cortés, V., M. Otero-Viñas, …, L. Badimon. 2002. Human coronary smooth muscle cells internalize versican-modified LDL through LDL receptor-related protein and LDL receptors. *Arterioscler. Thromb. Vasc. Biol.* 22:387–393.
20. Reference deleted in proof.
21. Tertov, V. V., A. N. Orekhov, …, V. N. Smirnov. 1992. Three types of naturally occurring modified lipoproteins induce intracellular lipid accumulation due to lipoprotein aggregation. *Circ. Res.* 71:218–228.
22. Tertov, V. V., I. A. Sobenin, …, A. N. Orekhov. 1989. Lipoprotein aggregation as an essential condition of intracellular lipid accumulation caused by modified low density lipoproteins. *Biochem. Biophys. Res. Commun.* 163:489–494.
23. Ismail, N. A., M. Z. Alavi, and S. Moore. 1994. Lipoprotein-proteoglycan complexes from injured rabbit aortas accelerate lipoprotein uptake by arterial smooth muscle cells. *Atherosclerosis.* 105:79–87.
24. Aviram, M., I. Maor, …, S. Milo. 1995. Lesioned low density lipoprotein in atherosclerotic apolipoprotein E-deficient transgenic mice and

in humans is oxidized and aggregated. *Biochem. Biophys. Res. Commun.* 216:501–513.

25. Llorente-Cortés, V., M. Otero-Viñas, …, L. Badimon. 2002. Low-density lipoprotein upregulates low-density lipoprotein receptor-related protein expression in vascular smooth muscle cells: possible involvement of sterol regulatory element binding protein-2-dependent mechanism. *Circulation.* 106:3104–3110.
26. Vijayagopal, P., J. E. Figueroa, …, Z. Tao. 1996. Marked alteration of proteoglycan metabolism in cholesterol-enriched human arterial smooth muscle cells. *Biochem. J.* 315:995–1000.
27. Frontini, M. J., C. O'Neil, …, J. G. Pickering. 2009. Lipid incorporation inhibits Src-dependent assembly of fibronectin and type I collagen by vascular smooth muscle cells. *Circ. Res.* 104:832–841.
28. Sandberg, L. B. 1976. Elastin structure in health and disease. *Int. Rev. Connect. Tissue Res.* 7:159–210.
29. Foster, J. A., L. Rubin, …, L. B. Sandberg. 1974. Isolation and characterization of cross-linked peptides from elastin. *J. Biol. Chem.* 249:6191–6196.
30. Li, B., and V. Daggett. 2002. Molecular basis for the extensibility of elastin. *J. Muscle Res. Cell Motil.* 23:561–573.
31. Debelle, L., and A. M. Tamburro. 1999. Elastin: molecular description and function. *Int. J. Biochem. Cell Biol.* 31:261–272.
32. Tamburro, A. M., A. Pepe, and B. Bochicchio. 2006. Localizing α-helices in human tropoelastin: assembly of the elastin "puzzle". *Biochemistry.* 45:9518–9530.
33. Floquet, N., S. Héry-Huynh, …, A. J. Alix. 2004. Structural characterization of VGVAPG, an elastin-derived peptide. *Biopolymers.* 76: 266–280.
34. Mecham, R. P. 1991. Introduction: catalyzing matrix stability. *Am. J. Respir. Cell Mol. Biol.* 5:205.
35. Samouillan, V., A. Lamure, …, M. Spina. 2000. Dielectric characterization of collagen, elastin, and aortic valves in the low temperature range. *J. Biomater. Sci. Polym. Ed.* 11:583–598.
36. Samouillan, V., C. André, …, C. Lacabanne. 2004. Effect of water on the molecular mobility of elastin. *Biomacromolecules.* 5:958–964.
37. Tintar, D., V. Samouillan, …, A. M. Tamburro. 2009. Human tropoelastin sequence: dynamics of polypeptide coded by exon 6 in solution. *Biopolymers.* 91:943–952.
38. Shi, G. P., G. K. Sukhova, …, P. Libby. 2003. Deficiency of the cysteine protease cathepsin S impairs microvessel growth. *Circ. Res.* 92:493–500.
39. Sukhova, G. K., Y. Zhang, …, G. P. Shi. 2003. Deficiency of cathepsin S reduces atherosclerosis in LDL receptor-deficient mice. *J. Clin. Invest.* 111:897–906.
40. Debelle, L., A. J. Alix, …, P. Legrand. 1998. The secondary structure and architecture of human elastin. *Eur. J. Biochem.* 258:533–539.
41. Bonnier, F., D. Bertrand, …, G. D. Sockalingum. 2008. Detection of pathological aortic tissues by infrared multispectral imaging and chemometrics. *Analyst (Lond.).* 133:784–790.
42. Hu, X., X. Wang, …, D. L. Kaplan. 2010. Biomaterials derived from silk-tropoelastin protein systems. *Biomaterials.* 31:8121–8131.
43. Dyksterhuis, L. B., E. A. Carter, …, A. S. Weiss. 2009. Tropoelastin as a thermodynamically unfolded premolten globule protein: the effect of trimethylamine N-oxide on structure and coacervation. *Arch. Biochem. Biophys.* 487:79–84.
44. Popescu, M. C., C. Vasile, and O. Craciunescu. 2010. Structural analysis of some soluble elastins by means of FT-IR and 2D IR correlation spectroscopy. *Biopolymers.* 93:1072–1084.
45. Tamburro, A. M., A. Pepe, …, I. P. Ronchetti. 2005. Supramolecular amyloid-like assembly of the polypeptide sequence coded by exon 30 of human tropoelastin. *J. Biol. Chem.* 280:2682–2690.
46. Salvi, A. M., P. Moscarelli, …, J. E. Castle. 2011. Influence of amino acid specificities on the molecular and supramolecular organization of glycine-rich elastin-like polypeptides in water. *Biopolymers.* 95:702–721.
47. Sionkowska, A., J. Skopinska-Wisniewska, …, A. Planecka. 2010. Chemical and thermal cross-linking of collagen and elastin hydrolysates. *Int. J. Biol. Macromol.* 47:570–577.
48. Barth, A. 2000. The infrared absorption of amino acid side chains. *Prog. Biophys. Mol. Biol.* 74:141–173.
49. Podet, E. J., D. R. Shaffer, …, J. R. Guyton. 1991. Interaction of low density lipoproteins with human aortic elastin. *Arterioscler. Thromb.* 11:116–122.
50. Hu, X. D. K., and P. Cebe. 2006. Determining β-sheet crystallinity in fibrous proteins by thermal analysis and infrared spectroscopy. *Macromolecules.* 39:6161–6170.
51. Krimm, S., and J. Bandekar. 1986. Vibrational spectroscopy and conformation of peptides, polypeptides, and proteins. *Adv. Protein Chem.* 38:181–364.
52. Debelle, L., A. J. Alix, …, P. Legrand. 1995. Bovine elastin and κ-elastin secondary structure determination by optical spectroscopies. *J. Biol. Chem.* 270:26099–26103.
53. Jackson, L. E., B. Faris, …, C. Franzblau. 1991. The effect of β-aminopropionitrile on elastin gene expression in smooth muscle cell cultures. *Biochem. Biophys. Res. Commun.* 179:939–944.
54. Samouillan, V., J. Dandurand-Lods, …, M. Spina. 1999. Thermal analysis characterization of aortic tissues for cardiac valve bioprostheses. *J. Biomed. Mater. Res.* 46:531–538.
55. Puett, D., A. Ciferri, …, J. Hermans, Jr. 1967. Helix formation of poly-L-lysine thiocyanate in aqueous solutions. *J. Phys. Chem.* 71:4126–4128.
56. Megret, C., A. Lamure, …, A. M. Tamburro. 1993. Solid-state studies on synthetic fragments and analogues of elastin. *Int. J. Biol. Macromol.* 15:305–312.
57. Hoeve, C. A., and P. J. Flory. 1974. The elastic properties of elastin. *Biopolymers.* 13:677–686.
58. Samouillan, V., J. Dandurand, …, M. Spina. 2012. Analysis of the molecular mobility of collagen and elastin in safe, atheromatous and aneurysmal aortas. *Pathol. Biol. (Paris).* 60:58–65.
59. Li, B., D. O. Alonso, and V. Daggett. 2002. Stabilization of globular proteins via introduction of temperature-activated elastin-based switches. *Structure.* 10:989–998.
60. Panagopoulou, A., A. Kyritsis, …, P. Pissis. 2011. Glass transition and dynamics in BSA-water mixtures over wide ranges of composition studied by thermal and dielectric techniques. *Biochim. Biophys. Acta.* 1814:1984–1996.
61. Frauenfelder, H., G. Chen, …, R. D. Young. 2009. A unified model of protein dynamics. *Proc. Natl. Acad. Sci. USA.* 106:5129–5134.
62. Cerveny, S., A. Alegria, and J. Colmenero. 2008. Universal features of water dynamics in solutions of hydrophilic polymers, biopolymers, and small glass-forming materials. *Phys. Rev. E.* 77:031803.
63. Samouillan, V., D. Tintar, and C. Lacabane. 2011. Hydrated elastin: dynamics of water and protein followed by dielectric spectroscopies. *Chem. Phys.* 385:19–26.